Engineering Fracture Mechanics 309 (2024) 110440

Contents lists available at ScienceDirect

Engineering Fracture Mechanics

journal homepage: www.elsevier.com/locate/engfracmech

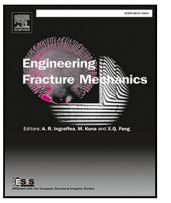

The role of the interfaces and cross-links on the mechanical behavior of mineralized collagen fibrils. A numerical approach

Ana Vercher-Martínez [a,*], Eugenio Giner [a], F. Javier Fuenmayor [a], J. Manuel García-Aznar [b]

[a] Instituto Universitario de Ingeniería Mecánica y Biomecánica - I2MB, Depto. de Ingeniería Mecánica y de Materiales, Universitat Politècnica de València, Camino de Vera, 46022 Valencia, Spain

[b] Group Multiscale in Mechanical and Biological Engineering (M2BE), Instituto Universitario de Investigación en Ingeniería de Aragón - I3A, Universidad de Zaragoza, C/María de Luna, 3, 50018 Zaragoza, Spain

ARTICLE INFO

Keywords:
Mineralized collagen fibril
Interfaces
Failure mechanisms
Cohesive law
Stiffness loss
Cross-link
Finite element method

ABSTRACT

Mechanical properties of bone tissue are highly dependent on its hierarchical structure. The presence of microcracks and diffuse damage in lamellar bone is correlated with the failure of the collagen-mineral interface in mineralized collagen fibrils (MCF). The main goal of this work is to evaluate the mechanical behavior of the interfaces and quantify the stiffness loss of the MCF associated with different failure mechanisms, under controlled in-plane displacement. Additionally, we aim to study the role of the cross-links on the fibril mechanical response, beyond the interface failure. Inter- and intra-microfibrilar cross-links are analyzed. In order to address the first issue, a detailed representative volume of the MCF is analyzed by means of the finite element method, under the assumption of plane strain and periodic boundary conditions. In this model the interfaces between constituents are modeled with an exponential cohesive law. Enzymatic cross-links, located at the molecular terminals connecting each 4D (D = 67 nm) staggered molecules, are represented by non-linear springs. Three in-plane controlled deformations are applied. The results of this work provide the anisotropic stiffness loss of the tissue involved in the different failure mechanisms at the nano-scale length. The initiation of microcracks and the presence of damage zones are compatible with the failure mechanisms observed at interfaces. Interface failure entails a progressive stiffness loss, bringing a non-linear behavior of bone. The strength obtained for the longitudinal maximum deformation is more than 20 times the transverse strength and 3.5 times the shear strength. The quantification of the reduction percentage in the elastic moduli and the shear stiffness when the fibril is damaged, has a potential application in improving failure criteria based on degradation of elastic constants. When longitudinal elongation is applied, the mechanical contribution of the cross-links in delaying the failure initiation of the interface is shown. Likewise, results of this work confirm the scarce influence of the cross-links in the strain range analyzed. Additionally, a three-dimensional numerical model of several microfibrils is defined with the aim of analyzing the mechanical relevance of inter- and intra-microfibrilar cross-links, beyond the interface failure. Results confirm that cross-links transfer the load when strain increases, being highlighted the mechanical competence of the trivalent cross-links.

* Corresponding author.
E-mail address: anvermar@dimm.upv.es (A. Vercher-Martínez).

https://doi.org/10.1016/j.engfracmech.2024.110440
Received 7 March 2024; Received in revised form 20 August 2024; Accepted 30 August 2024
Available online 3 September 2024

Table 1
Nomenclature of symbols used in the manuscript.

Symbol	Description
D	Periodical distance between staggered adjacent collagen molecules
L_c	Total length of the collagen molecule
L	Length of mineral platelet
T	Thickness of mineral platelet
V_f	Mineral volume fraction within the fibril
E_c, E_m	Young's modulus of collagen and mineral
ν_c, ν_m	Poisson's coefficient of collagen and mineral
T_n, T_t	Normal and tangential components of the surface traction
T	Surface traction vector
n, **t**	Unitary normal and tangential vector
Δ_n, Δ_t	Normal and tangential component of the surface separation
$\boldsymbol{\Delta}$	Surface separation vector
ϕ	Potential function
ϕ_n, ϕ_t	Work due to normal and tangential separation
σ_{max}, τ_{max}	Cohesive surface normal and tangential strength
δ_n, δ_t	Normal and tangential characteristics lengths
σ_{max}^{m-c}, τ_{max}^{m-c}	Cohesive surface normal and tangential strength fo mineral-collagen interaction
σ_{max}^{c-c}, τ_{max}^{c-c}	Cohesive surface normal and tangential strength fo collagen-collagen interaction
δ_n^{m-c}, δ_t^{m-c}	Normal and tangential characteristic lengths of mineral-collagen interaction
δ_n^{c-c}, δ_t^{c-c}	Normal and tangential characteristic lengths of collagen-collagen interaction
$D_{u,CL}$	Failure length of cross-links
F_x, F_y	Force components in x and y directions
d	Diameter of collagen molecule
ϵ_x, ϵ_y, γ_{xy}	Strain components in the two-dimensional problem
$^+$, $^-$	Symbols to denote opposite sides of the representative elemental volume
u, v	Displacement components in x and y directions
a, b, γ	Geometrical parameters of the microfibril quasi-hexagonal package
K_{CL}	Cross-link stiffness
E_x, E_y	Apparent elastic modulus in the x and y directions
G_{xy}	Apparent shear modulus in the xy plane
G_{col}	Shear modulus of collagen
ν_{xy}	Apparent Poisson's coefficient in the xy plane
Å	Amstron (unit)
D_x, D_y	Displacement components in x and y directions
K^{avg}	Averaged stiffness terms in x y and xy of the mineralized collagen fibril

Nomenclature of symbols used in the manuscript

In Table 1, the nomenclature and symbols used in the manuscript are summarized in order of their appearance.

1. Introduction

Mineralized type I collagen fibrils are the main structural component of bone tissue and their principal constituents are collagen, crystals of carbonated apatite (mineral) and water. Within the fibrils, adjacent collagen molecules are staggered along their long axis by $D = 67$ nm, giving the well known pattern of gap zones of ~ 35 nm length and overlap zones of ~ 32 nm length. Inside the fibrils, collagen forms a matrix that acts as a scaffold for the hierarchical mineralization process [1]. The mineral content (mineral volume fraction) and its geometrical distribution within the fibril are key aspects that contribute to the stiffness of the lamellar bone [2,3]. The staggered arrangement that collagen molecules follow in the axial direction of the fibrils is well established in the literature, e.g. [4–8]. In the transversal direction of the fibril, the crystals can coalesce to form large platelets across 3D channels formed by contiguous adjacent gaps that traverse the entire fibril [5,6]. In a cross-section to the longitudinal axis of the fibril, the collagen molecules in the fibril are arranged in a quasihexagonal packing [9]. The repetitive pentameric structures within the fibril are microfibrils and their interdigitating assembly throughout the intermicrofibrilar cross-links, forms the fibril [8,10].

The fibrous type I collagen is the most abundant in bone and its basic structure is a long (~300 nm), thin (~1.5 nm in diameter) protein that contains three coiled chains. A collagen molecule can be represented by five pseudo-periodic segments, where the periodic length D is considered as length measurement unit. The first four molecule segments are equal in length $D = 67$ nm and the fifth segment is approximately $0.47D$ in length, being the total length of the collagen molecule $L_c \approx 4.47D$. Molecules of collagen type I are flanked by telopeptides, the short non-helical regions. Segments 1 and 5 contain the nontriple helical telopeptides.

The molecular segments that contain the telopeptides are the potential locations for the enzymatic intermolecular cross-linking reactions. These covalent bonds are derived from aldehydes produced from lysyl and hydroxylysyl precursors by means of the enzyme lysyl oxidase. The immature enzymatic cross-links are divalent, i.e. they connect two molecules, and take place, per one collagen molecule, in four cross-linking locations, one in each telopetide and others two in specific sites of the triple helix. The immature cross-links in bone (mainly keto-imine) mature to form the pyridinoline (mainly Lysyl-pyridinoline) and pyrrole cross-links by further reaction of the keto-imine with telopeptide aldehydes [11]. The mature cross-links form a network of links in the fiber.

They stabilize the side-by-side interactions between collagen molecules. It has been postulated that the pyridinolines are divalent and the pyrroles are trivalent, and the presence of the later has been correlated with the mechanical competence of the tissue [12]. The mature cross-links could explain the increase of strength in bone with age despite of the reductions of immature cross-links but they are not replaced in all because of the activity of the continuum bone remodeling process. The mineralization process does not affect to the cross-link profile, rather that the post-translational modifications of the collagen is very important to the further mineralization [11].

Collagen molecules are stabilized by the formation of these strong cross-links between them. The mechanical strength of collagen fibrils is highly regulated by these intermolecular cross-links [13] since they prevent slippage under load. A rheological mechanical behavior for C-terminal in collagen type I is presented in [14].

Besides the precise enzymatic cross-links, the non-enzymatic or age-related cross-links occur as a result of reaction with glucose during ageing or diabetic disease and can cause tissue dysfunction as a consequence of the stiffening [15]. Intermolecular non-enzymatic cross-links are not located in specific sites. In the work of Buehler [16], atomistic and continuum studies are developed to characterize the nanomechanics of collagen fibrils considering different cross-links densities. It is proved that the relevance of the enzymatic cross-links is noticeable at large deformation regimes. In the work of Barkaoui and Hambli [17] the mechanical role of the cross-links is also evaluated showing a stiffer response of the structure as the cross-link density increases.

On the other hand, there are some studies in the literature that consider the mechanical influence of the interfaces between collagen molecules and also between collagen and mineral crystals of the mineralized collagen fibril. In [18] an exponential cohesive model is used to model the potential separation between boundaries and a cohesive model is also adopted for modeling the cross-links (enzymatic and non-enzymatic). In that work the mineral-collagen debonding is observed for the load case analyzed. In [19] the collagen-mineral interaction is modeled and the failure of interactions according to their nature is correlated with the presence of microcracks and diffuse damage in lamellar bone. These authors use a bi-linear cohesive law for representing the mineral-collagen interfaces. Both in the work of Siegmund et al. [18] and in the work of Luo et al. [19] a simplified model of the domain is considered and no quantification of the stiffness loss is discussed.

In the work of Hamed and Jasiuk [20] a multiscale damage and strength analysis is made by applying cohesive finite elements. In that work, related to the nano-scale level, the calculated strength of the mineralized fibril under longitudinal traction depends on the cell size and the type of interface. The model analyzed is similar to the presented in the work of Siegmund et al. [18] but includes different types of interfaces between mineral and collagen. In [21], a stability analysis of a bi-linear cohesive spring solution is considered to identify the crack initiation in nacre-like composite materials.

A molecular nano-mechanics approach of bone is presented in the work of Buehler [22]. By a combination of molecular dynamics and analytical analysis, the mineralized collagen fibril is analyzed. Interfaces are also modeled and his results provides values for the Young's modulus, yield strain and fracture stress in the longitudinal traction load case.

Despite full atomistic simulation is a very powerful method to simulate the nano-mechanical behavior of bone [10,14,23], it is far more expensive when several collagen molecules are included. An alternative is presented in the works of Buehler [16] and Depalle et al. [24], where a coarse-grain method is developed to deepen in the mechanical relevance of the enzymatic crosslinks in non-mineralized fibrils. Likewise, models based on strength of materials and micro-mechanics theories have been used to study the elastic behavior of bone at nano-structural level. An extensive review of all those procedures can be found in [25].

In the work of Fritsch et al. [26] the strength of bone is mainly related to the mineral-water interactions. The results of a multiscale continuum micromechanic model that includes ductile sliding between mineral crystals followed by the rupture of collagen crosslinks are compared with experimental micromechanics.

The finite element method is a numerical approach that has been applied in many works [17–19,23,27,28] to analyze the mechanical behavior of bone tissue at different length scales in a complementary or alternative way to the full atomistic simulation.

The main goal of this work is, firstly, to analyze the mechanical role of the interface constituents of the mineralized collagen fibril, determining the range of strain within they effectively act and quantifying the stiffness loss of the fibril as a consequence of interface failure. The different failure mechanisms involved are also identified. Secondly, we aim to analyze the influence of the cross-links beyond the interface failure, on the mechanical response of the microfibril, attending to the density and nature of the cross-links, i.e., inter- or intra-microfibrilar.

In order to achieve the first issue, a detailed two-dimensional model of the sub-microstructure under a plane strain assumption has been analyzed by the finite element method. Mineral crystals are modeled in the molecules gap zone. Collagen is divided into five sub-domains corresponding to five molecules. The interfaces between all constituents are modeled with an exponential cohesive law [18]. Furthermore, cross-links are modeled by a non-linear governing law as proposed by Uzel and Buehler [14]. The cross-links are established in the -N and -C terminals of each collagen molecule with the corresponding 4D staggered adjacent molecule.

A thorough study is provided to evaluate the response of the representative cell under three different load cases. Controlled deformations are applied for each of the x and y directions and for the shear load case.

In this work, the unit cell analyzed represents the mineralized collagen fibril following a staggered arrangement of the mineral crystals within the collagen fibril. Periodic boundary conditions ensure the periodicity of the cell. By making use of this model, the mechanical behavior of the mineralized collagen fibril under transversal traction and shear load is addressed and discussed. According to the authors' knowledge, this issue has not been reported in literature. In addition, enzymatic cross-links are modeled with a force–elongation non-linear relation. This idea was presented by Uzel and Buehler [14] but has not yet been applied using a finite element model; the results presented in this work provide, quantitatively, the amount of stiffness loss of the fibril for the load cases analyzed. The stiffness loss is also available in terms of the reduction of the apparent Young's moduli and shear modulus; likewise, strength limit ratios for the load cases analyzed are quantified and these can be useful to develop further failure criteria.

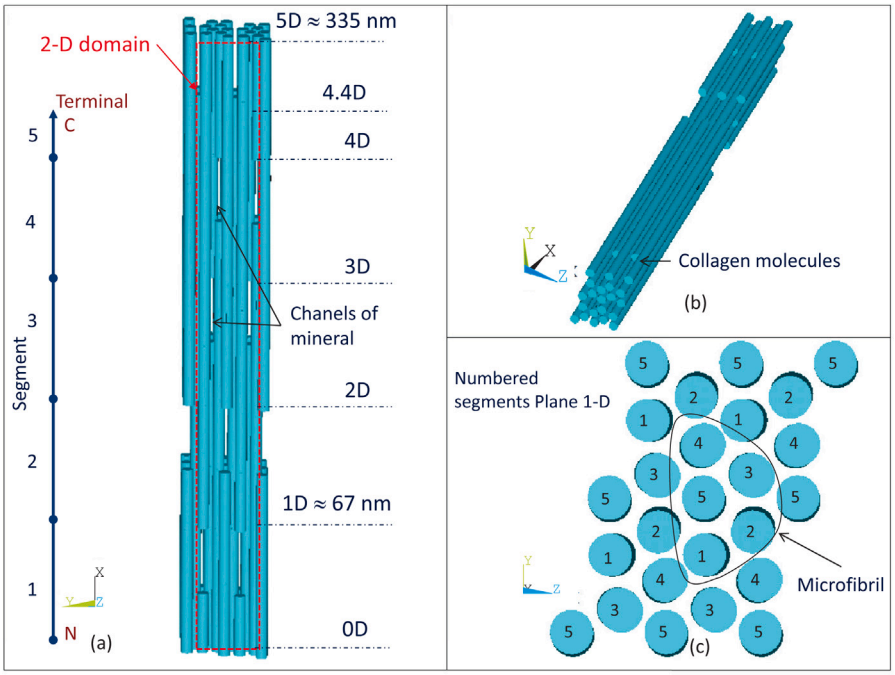

Fig. 1. (a) Three-dimensional schematic representation of several microfibrils distribution based on Orgel et al. [8,9]. Proportions are preserved, except that a scale factor of 0.2 has been applied in z direction to allow for an easier representation. This view shows the staggered arrangement of the collagen molecules and the locations where mineral crystals nucleate and grow through channels or grooves [30,31]. The scheme corresponds to a $5D$ model in length. In (b) an oblique view is depicted and in (c) a cross-sectional plane 1-D shows the numbered molecule segments. Dotted box in (a) points out the two-dimensional domain under a plane-strain assumption and in-plane periodic boundary conditions analyzed in this work.

In order to address the second issue, a three-dimensional finite element model of several pentameric collagen structure is developed basing on the Orgel's microfibril description [9]. In this model, both divalent and trivalent cross-links are included in specific sites and different densities. We aim to analyze the mechanical behavior of the fibril further the collagen molecules sliding as a consequence of the interface failure. In Section 2 the geometric of the two- and three- dimensional models, materials properties and the non-linear finite element model are described in detail. In Section 3 the most relevant results are presented for the load cases analyzed and finally, in Section 4, a discussion and conclusions of this work are provided.

2. Methods

2.1. Two-dimensional geometrical model description

In this work, a model of a representative cell of the mineralized collagen fibril has been considered according to the $5D$ ($D = 67$ nm) periodic model [29]. In Fig. 1, a schematic representation of the discrete three-dimensional model of several non-mineralized microfibrils is depicted. This figure is based on the works of Orgel et al. [8,9] applying a scale factor of 0.2 in z direction to allow for an easier representation.

In their works, a repetitive unit cell was identified and the molecular segments were highlighted through the 1D (overlap and gap) zone. Dotted box superimposed in Fig. 1a points out the simplified two-dimensional model analyzed in this work under a plane-strain assumption. The relationship between 3D and 2D models is based on two aspects: (1) Geometrical: discrete collagen molecules can be modeled as a two-dimensional collagen matrix implementing the interaction between molecules and mineral (see Fig. 2). On the other hand, mineral crystals are located in the gaps between adjacent molecules. These crystals can grow and coalesce in depth following the cavities between neighboring microfibrils. (2) Loading: lamellar tissue is made of successive sublayers within which fibrils orientation remain constant. Since the structural point of view, a lamella is a very thin structural component where membrane loads are predominant. At the microfibrils scale, it seems plausible to assume plane strain conditions. In Section 3.1.1 a comparative study of the elastic constants between the three-dimensional continuum model [3] and the two-dimensional of the present work is shown.

The dimensions of the mineral platelets are usual values found in the bibliography, $L = 50$ nm in length and $T = 3$ nm in thickness. A transversal overlapping of the mineral of 1.25 nm is enforced [3] to achieve a typical value of mineral volume fraction within the fibril, $V_f = 0.25$ [32]. The total dimensions of the 2-D domain analyzed are 335 nm in length and 8.75 nm in width. The selected geometrical boundaries guarantee a periodically repetitive structure.

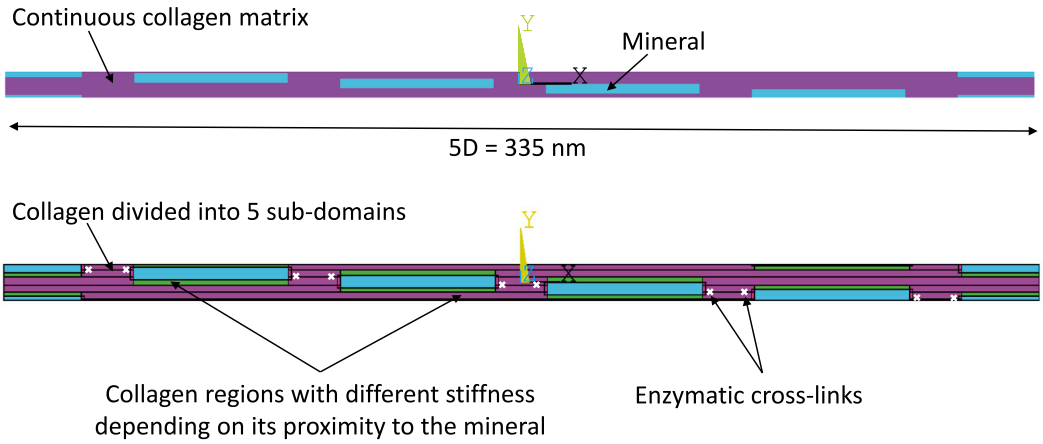

Fig. 2. Representative 2D-cell of a mineralized collagen fibril. The collagen matrix has been divided into five sub-domains and different Young's modulus are assigned to the collagen molecule by considering the mineral proximity and the direction of the applied load. Cross-links locations are marked with white crosses.

The Young's modulus for collagen has been modified depending on the collagen proximity to the mineral, following the work of Shashindra et al. [23] (see Fig. 2): $E_c = 2.95$ GPa and $\nu_c = 0.35$ in the central region of the molecule; the Young's modulus increases up to $E_c = 6.26$ GPa at the molecule terminals and $E_c = 13.17$ GPa in the molecule regions that interact laterally with minerals. The latter regions lie in the molecule segments adjacent to their terminals. According to Buehler [33], linear behavior for the collagen molecules is assumed in this work. For the isotropic elastic constants of the mineral, typical values are considered: $E_m = 114$ GPa and $\nu_m = 0.28$.

2.2. Two-dimensional finite element model

The model has been analyzed by means of the finite element method. Mineral platelets and collagen are modeled with bilinear quadrilateral elements with elastic behavior (see Fig. 3).

The constitutive law for the cohesive interfaces relates the traction and displacement across the surfaces. The normal T_n and tangential T_t components of the surface traction $\mathbf{T}$, $\mathbf{T} = \mathbf{n}T_n + \mathbf{t}T_t$ are obtained from the derivatives of the potential function ϕ (see Eq. (1)) with respect to the normal Δ_n and tangential Δ_t components of the surface separation $\boldsymbol{\Delta}$.

Considering the two dimensional problem, the potential function ϕ is defined as:

$$\phi(\Delta_n, \Delta_t) = \phi_n + \phi_n \exp\left(-\frac{\Delta_n}{\delta_n}\right)\left(-\left(1+\frac{\Delta_n}{\delta_n}\right)\exp\left(\frac{-\Delta_t^2}{\delta_t^2}\right)\right) \tag{1}$$

where $\phi_n = e\sigma_{max}\delta_n$ and $\phi_t = \sqrt{\left(\frac{e}{2}\right)}\tau_{max}\delta_t$ are the work of normal and tangential separation, respectively. Additionally, $e = exp(1)$, σ_{max} and τ_{max} are the cohesive surface normal strength and tangential strength, respectively, and δ_n and δ_t are the corresponding characteristic lengths.

Hence, T_n and T_t result:

$$T_n = -\sigma_{max}\frac{\Delta_n}{\delta_n}\exp\left(1-\frac{\Delta_n}{\delta_n}\right)\exp\left(\frac{-\Delta_t^2}{\delta_t^2}\right) \tag{2}$$

$$T_t = -2\frac{\delta_n}{\delta_t}\sigma_{max}\frac{\Delta_t}{\delta_t}\left(1+\frac{\Delta_n}{\delta_n}\right)\exp\left(1-\frac{\Delta_n}{\delta_n}\right)\exp\left(\frac{-\Delta_t^2}{\delta_t^2}\right) \tag{3}$$

In Eqs. (2)–(3) it is assumed that the normal work and the shear work of separation are equal and the normal separation is neglected after total shear decohesion, with $T_n = 0$ [34].

In [19], a bilinear cohesive law is used to model all the interfaces between the constituents of the mineralized collagen fibril, but it is stated that only collagen-mineral interface fits to that model, being more convenient to use an exponential law for the other interactions (collagen-collagen).

In our model, the exponential cohesive law proposed by Xu and Needleman [35] is used for all interactions, following Siegmund et al. [18]. In Fig. 3, the different cohesive interfaces are depicted. The critical parameters can be summarized in the following values: at the mineral-collagen interface a structural water provides a strong interaction between constituents being the cohesive surface normal strength $\sigma_{max}^{m-c} = 270$ MPa and the normal characteristic length $\delta_n^{m-c} = \delta_t^{m-c} = 0.2$ nm. At the collagen-collagen interface a weak interaction is provided mainly by the electrostatic forces being the normal strength $\sigma_{max}^{c-c} = 30$ MPa and the normal characteristic length $\delta_n^{c-c} = \delta_t^{c-c} = 1$ nm [18]. The shear strength τ_{max} is related with σ_{max} by means of $\tau_{max} = \sqrt{2e}\sigma_{max}$. In Fig. 4 the

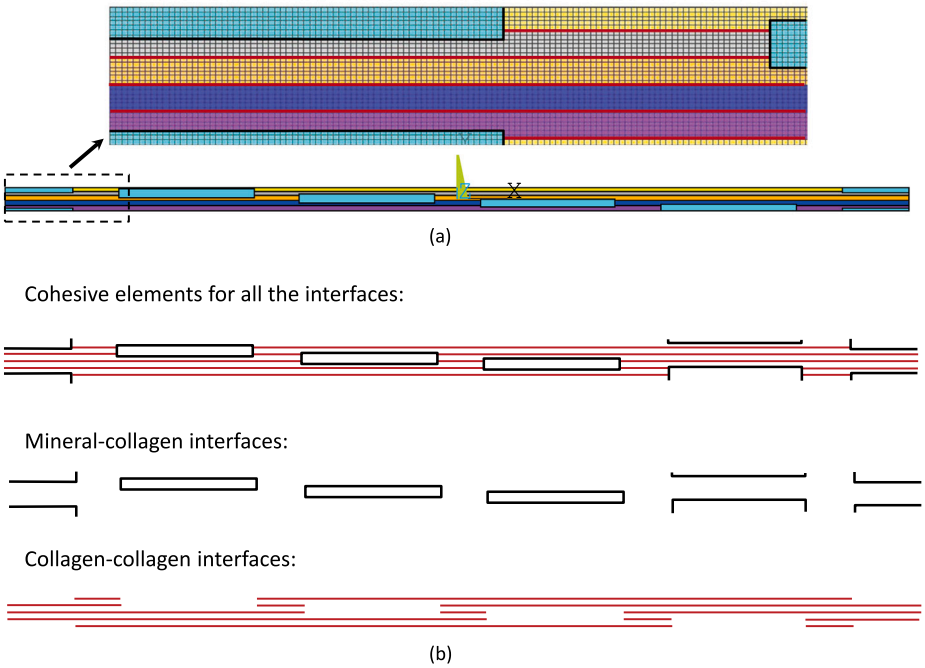

Fig. 3. (a) Detail of the model mesh where cohesive elements have been used for the constituents interfaces. (b) Cohesive elements for mineral-collagen interfaces (in black) and for collagen-collagen interfaces (in red).

cohesive traction T_t given by Eq. (3) is depicted considering the cohesive parameters for the collagen-collagen molecules interface. The maximum value of $T_t = \tau_{max}$ is achieved when $\Delta_t = \sqrt{2}\delta_t^{c-c}/2$.

Enzymatic cross-links have been modeled through non-linear springs elements that are placed between each 4-D staggered collagen molecule, connecting each terminal (N and C) with the adjacent helix zone. For each collagen molecule, these elements are located at the four potential sites for cross-link lysyl oxidasa mediated. These locations are marked with white crosses in Fig. 2. In the work of Uzel and Buehler [14] a non-linear rheological model for the mechanical behavior of the C-terminal cross-links domain in type I collagen is proposed. In this work, the numerical model includes both the linear elastic response of the cross-links and the regime corresponding to the unrolling of the telopeptide. As can be seen in Fig. 4, function in blue, the elongation corresponding to the unrolling of the telopeptide and the molecules sliding at the terminals is assumed 2 nm [14]. This implies a delay in the cross-link response. Following this point, a new elongation of 1 nm is considered to model the phase stretching-elongation of the cross-link before its forward rupture [18]. The force needed to produce the cross-link failure depends mainly on the maximum capability for supporting the load of C–C and C–N bonds and, in turn, this force depends on the duration of the load application [36]. The load must be transferred through the area of influence of the cross-link and that is estimated as $D/200 \times d$ with d being the molecule diameter [18]. By considering the element length in the numerical model (≈ 0.25 nm), two elements are selected at each specific site and connected by means of three parallel non-linear springs (one per node).

In order to obtain the global stress–strain relation of the system, displacement controlled analyses have been performed. The in-plane load cases analyzed are independent tensile tractions in the x and y direction and a shear load. For each load case, boundary conditions guarantee the consideration of one strain component exclusively: ϵ_x, ϵ_y and γ_{xy}. Proper constraint equations and Dirichlet boundary conditions ensure the periodicity of the domain in the orthogonal direction of the applied elongation loads and in the longitudinal direction for the shear load case. Regarding these periodic boundary conditions, we have simulated an infinitely large fibril in the direction where periodicity is applied [22]. Fig. 5 shows, schematically, the three load cases and periodic boundary conditions applied in a generic 2-D elastic domain of dimensions L and W. Opposite sides are designed with superscripts $^+$ and $^-$. The following equations summarize the approach for applying the controlled deformations in the numerical model:

$$\epsilon_x = \frac{u^{1^+} - u^{1^-}}{L} \tag{4}$$

$$\epsilon_y = \frac{v^{2^+} + v^{2^-}}{W} \tag{5}$$

$$\gamma_{xy} = \frac{u^{2^+} - u^{2^-}}{W} + \frac{v^{1^+} - v^{1^-}}{L} \tag{6}$$

In load case 1, $u^{1^-} = 0$ and u^{1^+} is gradually applied to impose $\epsilon_x \neq 0$. In addition, $v^{2^+} = v^{2^-}$, $u^{2^+} = u^{2^-}$ and $v^{1^+} = v^{1^-}$ to get $\epsilon_y = \gamma_{xy} = 0$.

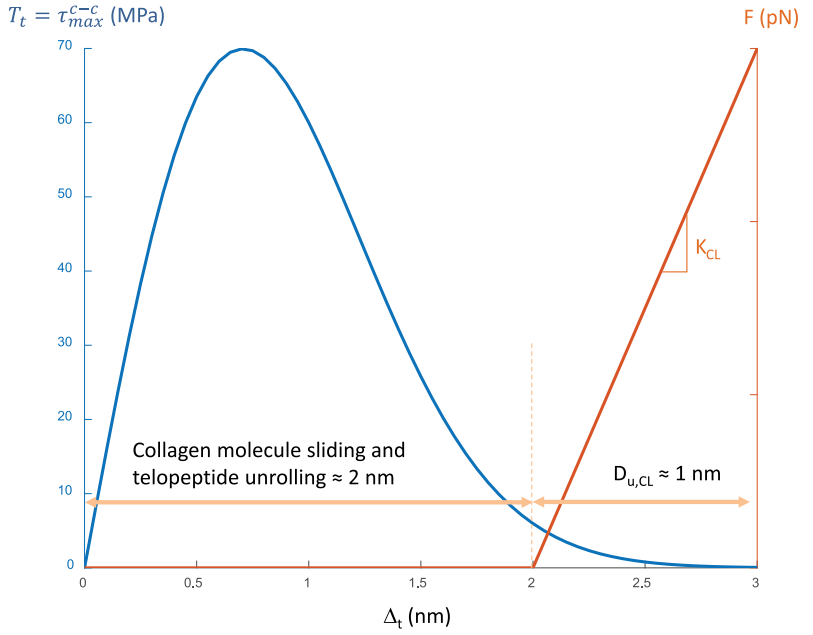

Fig. 4. Function in blue: shear stress T_t following the exponential cohesive law given in Eq. (3) with the cohesive parameters for the collagen-collagen molecules interface. In this case, $\delta_t^{c-c} = 1$ nm and $\sigma_{max}^{c-c} = 30$ MPa, hence $\tau_{max}^{c-c} = 70$ MPa. Function in red: force–elongation function for the non-linear spring to consider first the sliding between collagen molecules as a consequence of the telopeptide unrolling (delay) and next the linear elastic response of the cross-link.

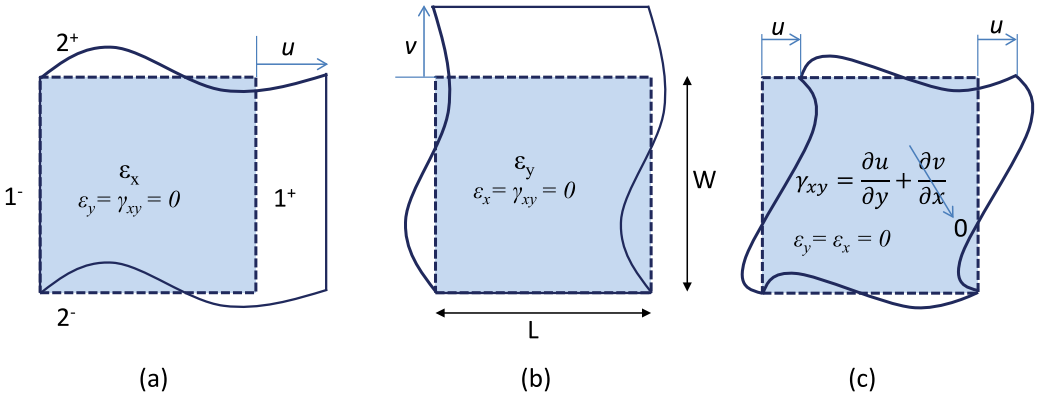

Fig. 5. Schematic representation of the load cases with periodic boundary conditions in the orthogonal direction of the elongation load cases (a), (b) and in the longitudinal direction for the shear load case (c).

In load case 2, ϵ_y is applied with $v^{2^-} = 0$ and controlled v^{2^+}. The rest of components are zero by means $u^{1^+} = u^{1^-}$, $u^{2^+} = u^{2^-}$ and $v^{1^+} = v^{1^-}$.

Finally, in load case 3, $v^{1^+} = v^{1^-}$, $u^{2^-} = 0$ and u^{2^+} is progressively increased to apply $\gamma_{xy} \neq 0$. Simultaneously, $u^{1^+} = u^{1^-}$, $v^{2^+} = v^{2^-}$ produce $\epsilon_x = \epsilon_y = 0$.

This procedure leads to periodic stress components in the periodic boundaries, $\sigma_i^+ = \sigma_i^-$.

2.3. Three-dimensional geometrical model description

In order to consider the spatial distribution of the inter- and intra- cross-links on the mechanical response of collagen fibrils, a three-dimensional analysis basing on Orgel et al. [9] has been developed. Microfibrils are structured in a quasi-hexagonal package in a monoclinic lattice, being $a = 4$ nm, $b = 2.7$ nm and $\gamma = 105.6^o$ (see Fig. 6). Collagen molecules have been created following by a right-hand helically twisted function [37].

The segments of the collagen molecules have been schematically depicted in Fig. 7. Note that microfibril is constituted by a $5D$ periodic unit where both inter- and intra-microfibrilar cross-links ensure an interrelated microfibrils network and provide the mechanical stability of the fiber structure. Non-enzymatic cross links are established between $1D$ staggered molecules while

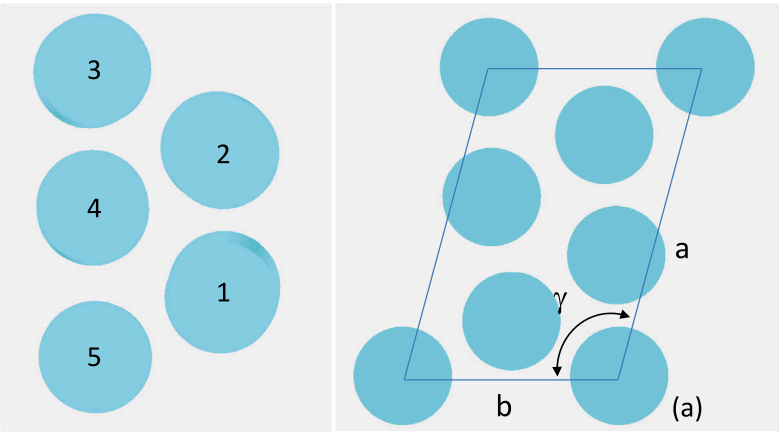

Fig. 6. Microfibril quasi-hexagonal package in a monoclinic lattice.

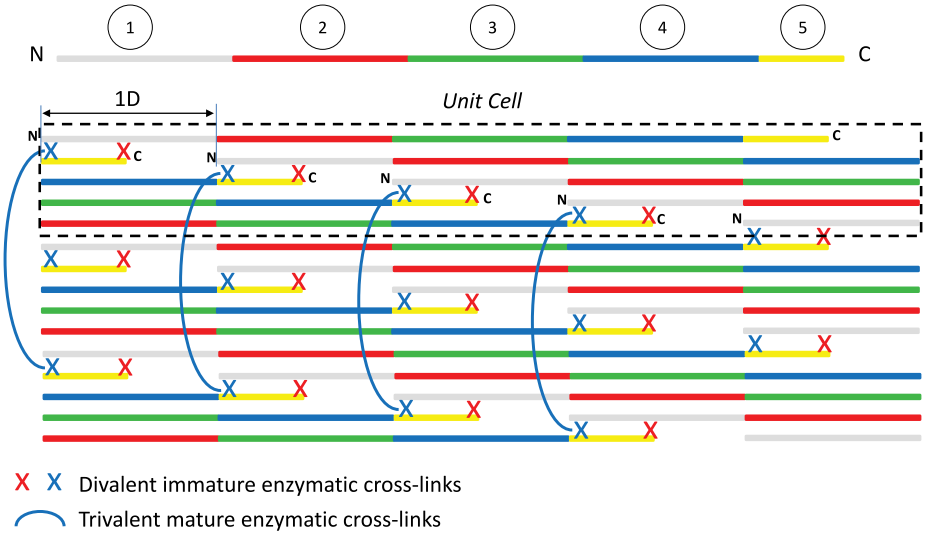

Fig. 7. Divalent and trivalent cross-links represented in the Hodge–Petruska's model. Trivalent cross-links take place at N-terminal and they connect molecules of different microfibrils. On the other hand, divalent cross-links are represented with crosses and are located between 4D staggered molecules in the overlap zone.

enzymatic cross links take place between $4D$ staggered molecules. Each collagen molecule is connected to others by, at least, four points: in N-terminal, in C-terminal and two others at specific sites of the three α chains of the collagen molecule.

In Fig. 8 the position of the inter-microfibrilar cross-links in different planes is depicted. Intra-microfibrilar cross-links are highlighted in red on the microfibril spatial view. The final model is obtained by replicating this unitary microfibril.

2.4. Three-dimensional finite element model

The collagen molecules have been meshed with hexahedral solid lineal elements and a non-linear elastic model has been used for the cross-links, which force–elongation relationship follows the function in red shown in Fig. 4. Elastic properties for collagen are $E_{col} = 2.95$ MPa and $\nu_{col} = 0.35$ and the cross-link stiffness is $K_{CL} = 1181.43 \times 10^{(-11)}$ N/nm [16].

In Fig. 9 the three-dimensional model with details of the mesh is shown.

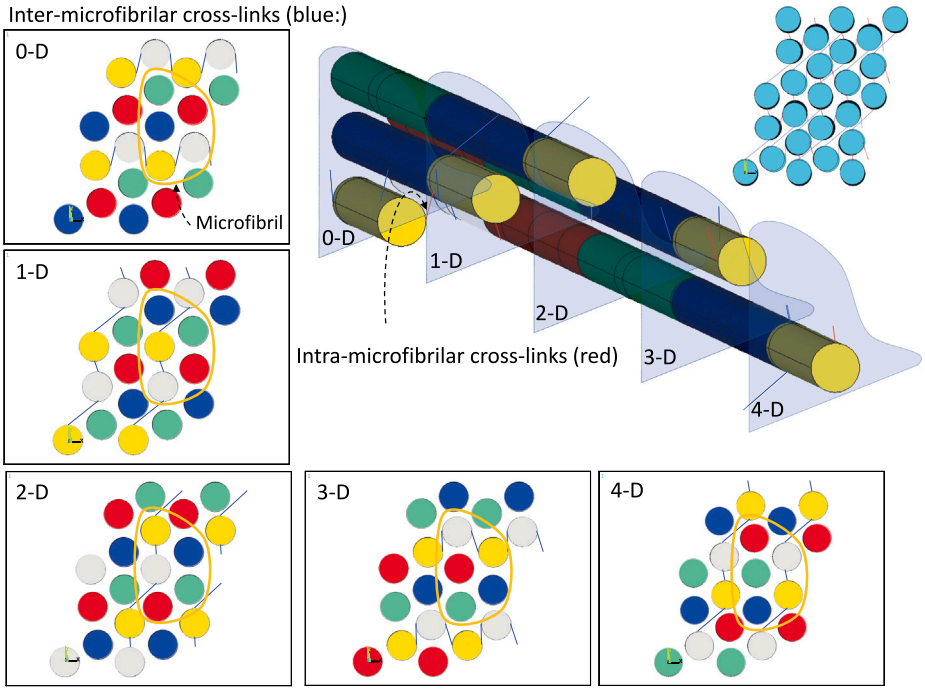

Fig. 8. Geometrical model of the pentameric unit or microfibril. For the shake of clarity, a scale factor of 0.2 in the longitudinal direction has been applied. Inter- and intra-microfibrilar cross-links are also depicted.

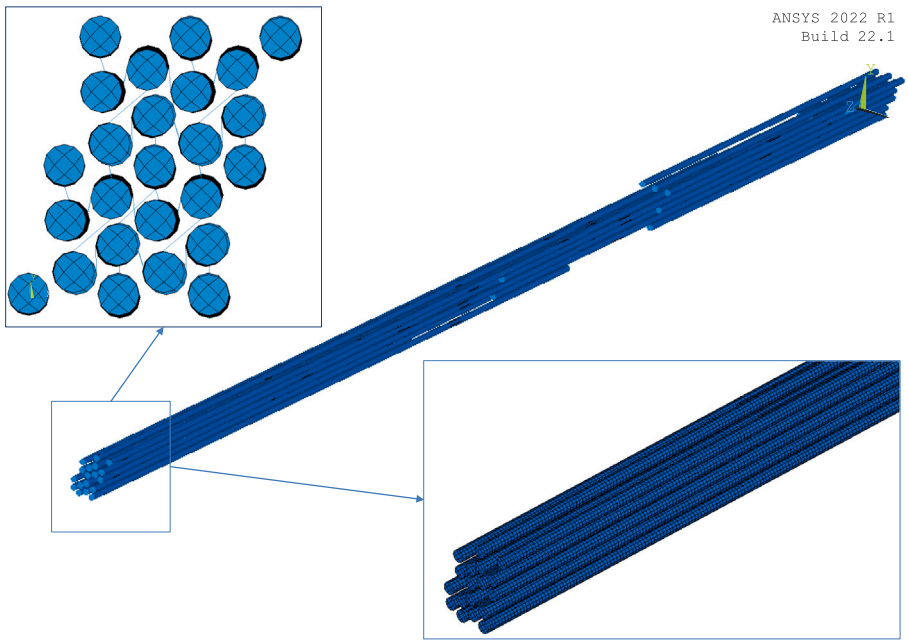

Fig. 9. Three-dimensional numerical model of microfibrils with inter- and intra-microfibrilar cross-links.

Table 2
Normalized elastic constants and the difference (%) between the homogenized elastic constants estimated with the three-dimensional model [3] and two-dimensional plane-strain model (present work).

	3-D model	Plane-strain model	Error (%)
	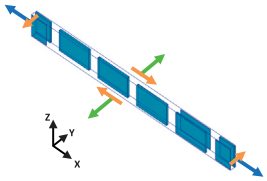	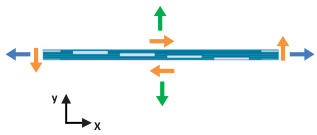	
E_x/E_{col}	4.426	4.484	+1.29
E_y/E_{col}	1.909	2.030	+6.33
G_{xy}/G_{col}	1.361	1.370	+0.66
ν_{xy}/ν_{col}	1.106	1.240	+12.12

3. Results

3.1. Analysis of the mechanical role of the microfibril interfaces under two-dimensional plane-strain assumption

In this section, firstly, the equivalence between a three-dimensional approach [3] and the plane-strain behavior assumed in this work (see Section 2) is analyzed in order to estimate the elastic constants of the mineralized collagen fibril. Subsequently, the results for the in-plane load cases will be presented.

3.1.1. Equivalence between three-dimensional and two-dimensional models for elastic behavior

The sharing features between the two models are the following: (1) the $5D$ periodic arrangement (with $D = 67$ nm) is considered, (2) the collagen matrix is idealized as a continuum with uniform elastic constants along the molecule length, (3) an identical geometrical disposition of the constituents (including mineral overlapping) is adopted, (4) the same elastic properties and dimensions of the minerals are included and, (5) neither cohesive interfaces nor cross-links are modeled so that all interfaces are assumed to be perfectly bonded. The elastic constants to be compared are estimated using the finite element method by means of a direct numerical homogenization procedure [3].

As expected, results shown in Table 2 point out that the two-dimensional model provides a slightly stiffer behavior. Under the assumption of a plane strain condition the two dimensional model fits with mineral growth in the transverse direction of the fibril compatible with the mineral channels or grooves observed by Landis and Song [30]. Results show a 1.29% error in the normalized elastic modulus in the longitudinal direction of the microfibril and 0.66% in the in-plane shear modulus. Difference in the transverse modulus is higher (6.33%). Variations in the Poisson's ratios estimation are no significant in the global mechanical response. One can conclude that results are admissible and, for the main goal of this work, the 2D plane strain model is adopted.

3.1.2. Load case 1: ϵ_x

In this section and Sections 3.1.3–3.1.4, the numerical models analyzed are the following: (1) *Continuous interfaces*, where no cohesive model is used, that means a perfect contact between mineral and collagen molecules, for this model the stiffest results will be always expected, (2) *Collagen*, in this model no mineralization is consider, as in (1) the contact between collagen molecules is always bonded, (3) *Cohesive interfaces*, where all the interactions between the constituents are modeled by means of Eqs. (2) and (3). (4) *Cohesive interfaces and enzymatic cross-links*, in this model non-linear springs are added to the model (3) in order to include the incipient action of the cross-links.

In this section, the results corresponding to the imposed deformation in the x-direction, ϵ_x, are shown. The x-direction of the model coincides with the longitudinal direction of the fibril.

In Fig. 10 the deformed shape of the structure under the maximum strain analyzed is depicted. It shows debonding of the collagen-mineral interface normal to the load direction, providing zones where microcracks can initiate. Sliding is also observed at the interface between collagen molecules, specially at the ends where the shear stress is higher.

This local bending is offset by the action of the cross-links. The eccentric force that the cross-links provide introduce a balance moment into the collagen molecule. That behavior is observed in both molecule terminals.

Another interesting result is that the gap and overlap regions show different behavior. Because the Poisson's ratio of collagen is higher than that of the mineral, molecules in the overlap regions tend to stretch themselves, leading to normal debonding between collagen molecules.

In Fig. 11 the normalized value of the stress in x-direction σ_x/E_{col} is shown as a function of the applied strain ϵ_x. The scaling Young's modulus considered is the corresponding to the central zone of the molecule $E_{col} = 2.95$ GPa. One can note that the inclusion of the debonding interfaces leads to a very high influence on the model apparent stiffness. If we compare the circle-marked results with the upper solid line for the model with continuous interfaces, the loss of stiffness is evident due to the inclusion of the cohesive governing law at the interfaces and the corresponding debonding. Up to $\epsilon_x = 0.02$, what implies an overall displacement near

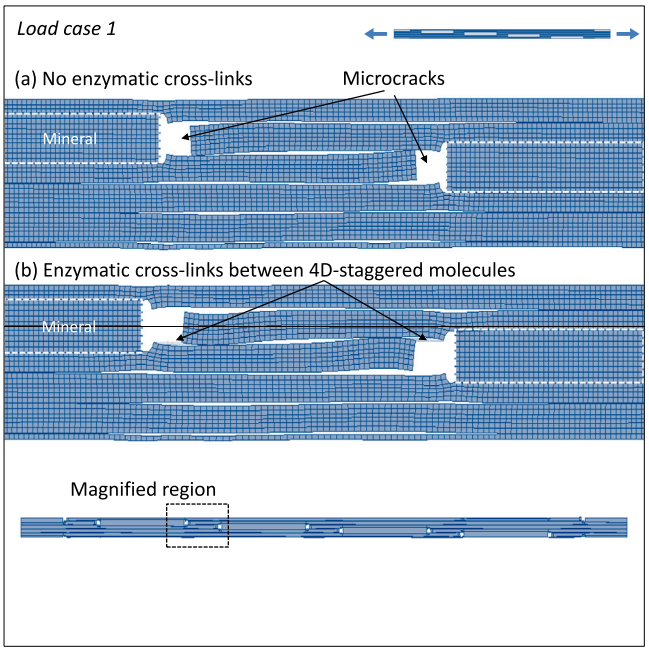

Fig. 10. Load case 1: ϵ_x. Deformed shape when maximum strain is applied in x-direction. In the magnified region (inset), the failure of cohesive interfaces between collagen and mineral is shown: (a) absence of cross-linking, (b) the enzymatic cross-links are included.

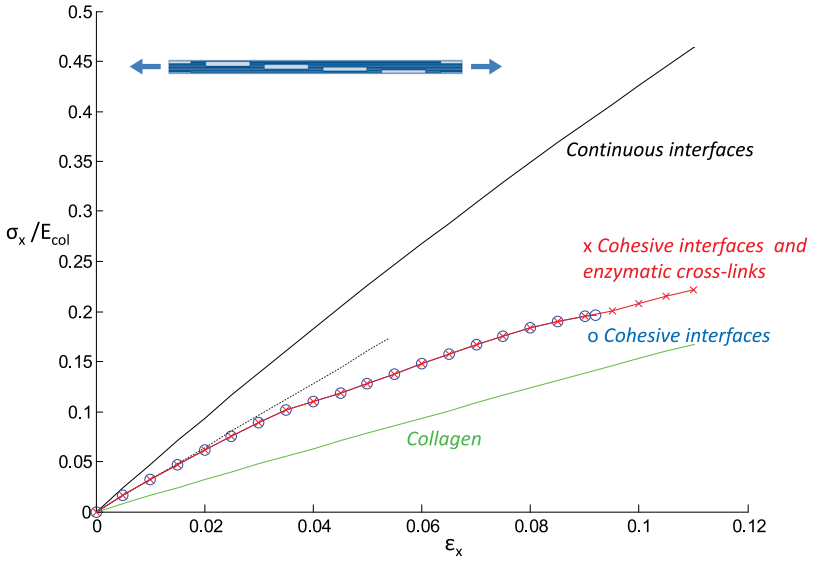

Fig. 11. Evolution of the normalized stress in x-direction, σ_x/E_{col}, with the strain ϵ_x for the following models: continuous interfaces; cohesive interfaces and enzymatic cross-links; cohesive interfaces; collagen without mineral.

50 Å (see Fig. 12), the behavior is still linear (dotted line), but from that point on, a non-linear behavior governs the mechanical response due principally to the incipient sliding between collagen molecules.

Cohesive interfaces fail when the applied strain is near $\epsilon_x = 0.092$. At this point, the relative displacement measured in the numerical model between nodes connected by the non-linear springs (cross-links) is slightly higher than 2 nm, so complete sliding between collagen molecules and telopeptide unrolling is achieved, then, the cross-links begin to work (see Fig. 4). This can be observed in the results with x-marks of Fig. 11.

In Fig. 12 the evolution of the resultant force in x-direction with the displacement in the same direction is depicted. As a consequence of the progressive normal debonding failure, the stiffness loss in the longitudinal direction undergoes a drop of 32.4%, from 24.7 pN/Å (slope of the upper dotted line) to an average stiffness for the non linear behavior of 16.7 pN/Å.

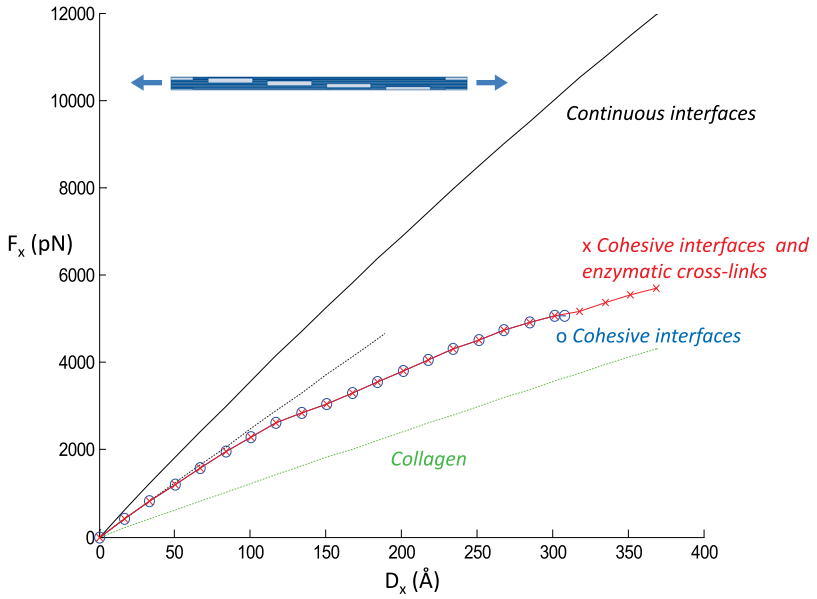

Fig. 12. Evolution of the resultant force F_x (pN) with the displacement applied D_x (Å) for the following models: continuous interfaces; cohesive interfaces and enzymatic cross-links; cohesive interfaces; collagen without mineral.

3.1.3. Load case 2: ϵ_y

In this section, the results obtained from the controlled deformation in y-direction are presented. The y-direction in the model corresponds to a transverse direction of the mineralized collagen fibril.

In Fig. 13 the deformed shape of the model indicates that the load applied causes the debonding in the normal direction to the collagen molecules interfaces. As described in Section 2, these interfaces are the weakest and, for the direction of the applied strain, they are in a series configuration. Therefore this brings the most unfavorable situation. The mineral-collagen interfaces avoid the total failure of the structure while the cohesive strength is not exceeded. Cross-links slightly prevent the normal separation between terminals (see arrow ends in Fig. 13b) but no specific relevance is observed in the global mechanical response of the model.

In Fig. 14 the normalized value of the stress in y-direction σ_y/E_{col} is shown as a function of the applied strain ϵ_y. As in Section 3.1.2, the scaling Young's modulus considered is the corresponding to the central zone of the molecule $E_{col} = 2.95$ GPa. As expected, if the interfaces between constituents are perfectly bonded (upper solid line), the global stiffness in y-direction is governed by the matrix stiffness. In this case the collagen (upper dotted curve). But, when the constituents interfaces are included (circle-marked results) an evident loss of stiffness in y-direction of the model takes place.

For this load case, the linear regime extends close to $\epsilon_y = 0.05$, what implies a displacement slightly lower than 5 Å (see Fig. 15). From this point on, the behavior becomes non-linear. For this analysis no special contribution of the enzymatic cross-links is observed.

If we compare Figs. 11 and 14 when interfaces fail, the stress in the fibril is more than 20 times higher in its longitudinal direction than in the transverse direction.

Analogously to the results shown in Fig. 12, the evolution of the resultant force in y-direction with the displacement in the same direction is depicted in Fig. 15. The normal debonding between collagen molecules implies a stiffness loss in the transverse direction of 54.8%, from 804.14 pN/Å (slope of the lower dotted line) to an average stiffness for the non-linear behavior of 362.06 pN/Å.

3.1.4. Load case 3: γ_{xy}

In this section, the mechanical response of the structure analyzed for a controlled shear deformation γ_{xy} is detailed.

In Fig. 16 the deformed shape corresponds to the last level of shear strain applied. In this case, the failure is produced by the complete sliding of collagen molecules. Because the shear modulus of the collagen is less than the mineral, a higher angular distortion is produced in the overlap collagen zone. For this load case, no special influence of the enzymatic cross-links is observed in the range of γ_{xy} analyzed.

In Fig. 17 the normalized value of the shear stress in xy-plane τ_{xy}/G_{col} is shown as a function of the applied shear strain γ_{xy}. The scaling shear modulus considered is obtained from the isotropic assumption, being Young's modulus $E_{col} = 2.95$ GPa and Poisson's coefficient $\nu_{col} = 0.35$. Analogous to Section 3.1.3 the mechanical response of the model with continuous interfaces (upper solid line) is completely influenced by the collagen matrix (upper dotted line). When cohesive interfaces are added to the model, the behavior differs significatively becoming more compliant. For this load case, the strain range for which the linear regime is valid gives the maximum amplitude for the three load cases analyzed and progressively becomes non-linear as the interfaces slide.

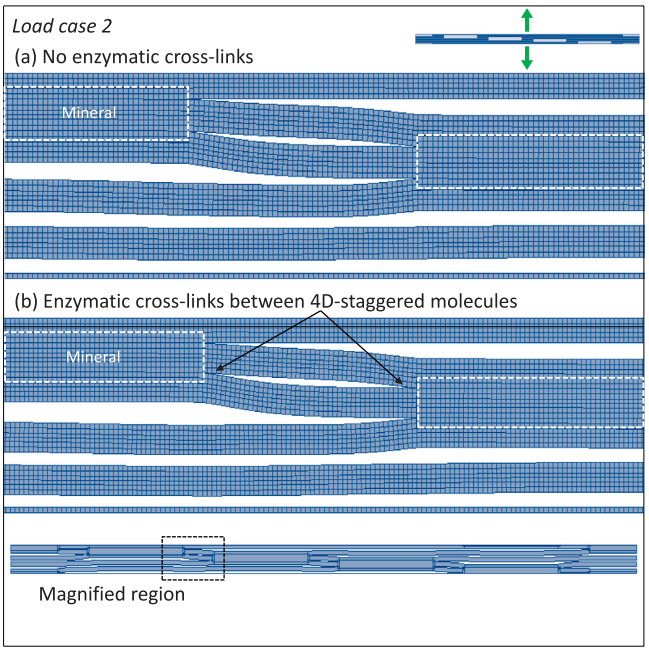

Fig. 13. Load case 2: ϵ_y. Deformed shape when maximum strain is applied in y-direction. In the magnified region (inset) the failure of cohesive interfaces between collagen sub-domains is shown: (a) no enzymatic cross-links, (b) enzymatic cross-links are included.

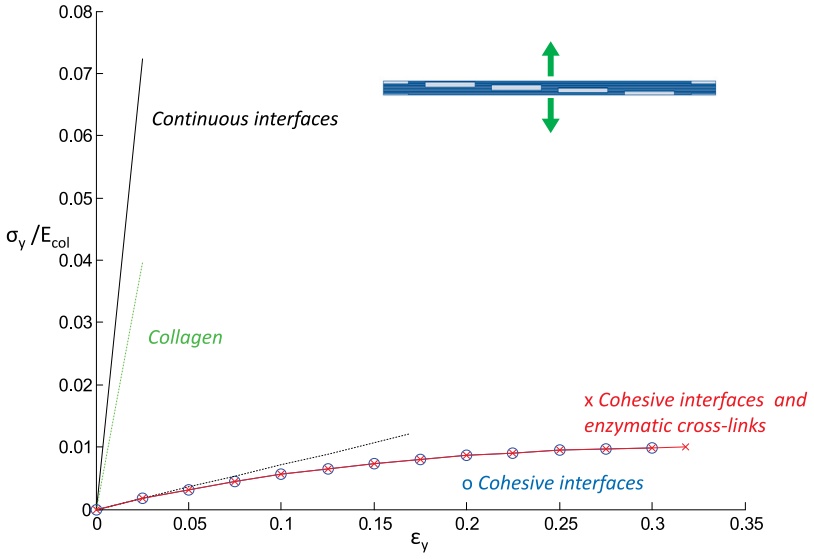

Fig. 14. Evolution of the normalized stress in y-direction, σ_y/E_{col}, with the strain ϵ_y for the following models: continuous interfaces; cohesive interfaces and enzymatic cross-links; cohesive interfaces; collagen without mineral.

If we compare results from Figs. 11 and 17, the maximum tensile load that can carry the fibril in its longitudinal direction is at least 3.5 times greater than the maximum shear stress in the transverse plane defined by the mineral dimensions L (length) and T (thickness).

In Fig. 18 the evolution of the resultant shear force in xy-plane with the displacement in x-direction is represented. For the in-plane shear strain applied, the failure mechanisms are based on the progressive sliding of collagen molecules. In this case, the stiffness loss is 19%, from 1355.6 pN/Å (slope of the lowest dotted line) to an average stiffness for the non-linear behavior of 1097.6 pN/Å.

A results summary is provided in Table 3. All the models include the non-linear geometric feature. As expected, the model with continuous interfaces provides the upper bound for the estimated stiffness of the mineralized collagen fibrils. When the cohesive law

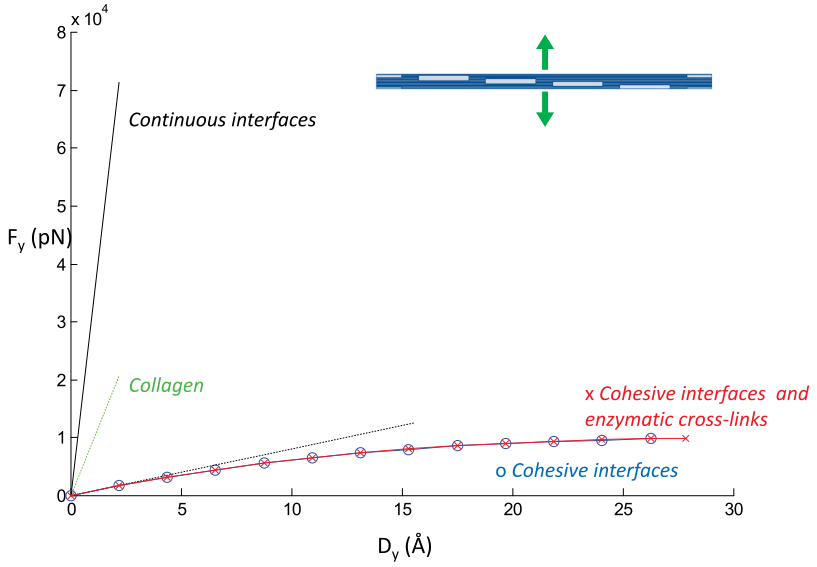

Fig. 15. Evolution of the resultant force F_y (pN) with the displacement applied D_y (Å) for the following models: continuous interfaces; cohesive interfaces and enzymatic cross-links; cohesive interfaces; collagen without mineral.

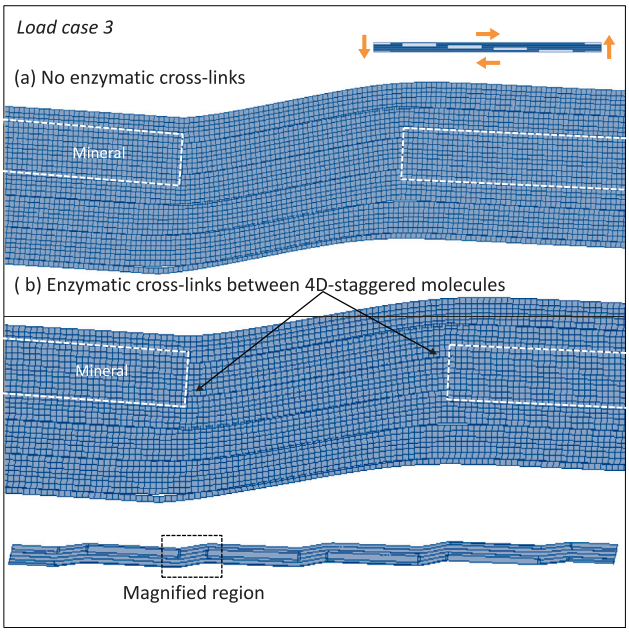

Fig. 16. Load case 3: γ_{xy}. Deformed shape when maximum shear strain is applied in xy-plane. In the magnified region (inset), the failure of cohesive interfaces between sliding collagen sub-domains is shown: (a) no enzymatic cross-links, (b) enzymatic cross-links are included.

is added to model the interactions between constituents at interfaces, stiffness is significantly reduced, specially in the transverse direction and shear modulus. If load increases up to the interface failure, stiffness will be progressively reduced as well. When cohesive interfaces are modeled, the linear behavior range depends on the load applied: for the longitudinal traction, the linear response is observed for $\varepsilon \leq 0.02$ and for the transverse traction and shear load, for $\varepsilon \leq 0.05$. The apparent Young's modulus for each direction and the shear modulus are estimated from the averaged stiffness in the strain range analyzed following the next equations:

$$E_x^{avg} = \frac{K_x^{avg} L}{W} \tag{7}$$

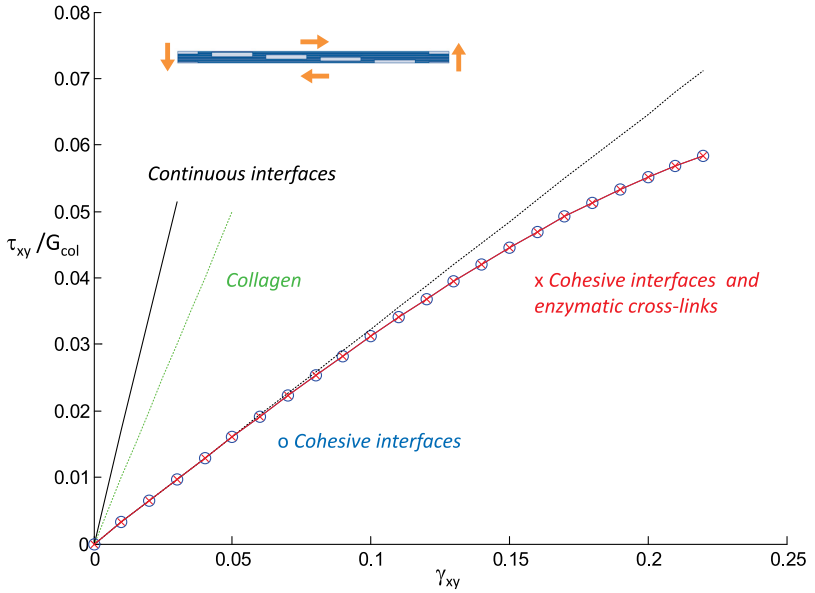

Fig. 17. Evolution of the scaled shear stress in xy-plane, τ_{xy}/G_{col}, with the shear strain γ_{xy} for the following models; continuous interfaces; cohesive interfaces and enzymatic cross-links; cohesive interfaces; collagen without mineral.

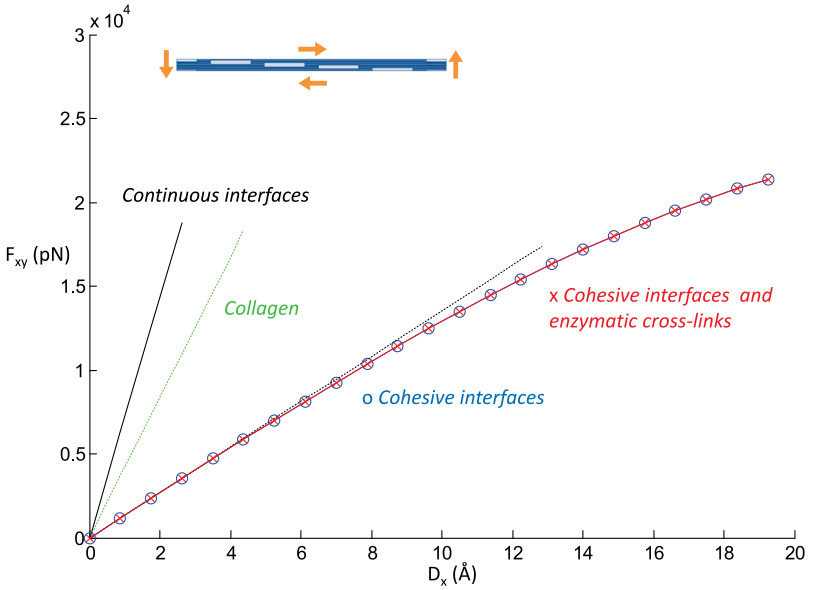

Fig. 18. Evolution of the resultant shear force F_{xy} (pN) with the displacement applied D_x (Å) for the following models: continuous interfaces; cohesive interfaces and enzymatic cross-links; cohesive interfaces; collagen without mineral.

$$E_y^{avg} = \frac{K_y^{avg} W}{L} \tag{8}$$

$$G_{xy}^{avg} = \frac{K_{xy}^{avg} W}{L} \tag{9}$$

where the domain dimensions are L and W (see Fig. 5) and unit thickness has been assumed.

Table 3
Estimated stiffness K, homogenized Young's moduli and shear stiffness for mineralized collagen fibril.

	K_x^{avg}	E_x^{avg}	K_y^{avg}	E_y^{avg}	K_{xy}^{avg}	G_{xy}^{avg}
Continuous interfaces[a]	33.33	12.76	26 562	6.94	7244.3	1.892
Cohesive interfaces	24.71	9.46	804.14	0.209	1355.6	0.354

Units: pN/Å(K), GPa (E, G).
[a] Upper bounds.

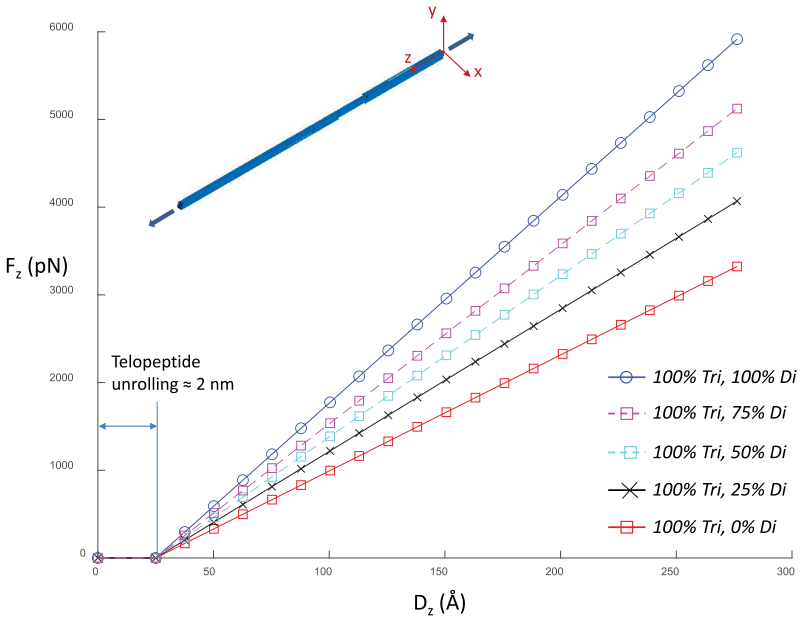

Fig. 19. Evolution of the reaction force F_z (pN) with the displacement applied D_z (Å), considering different values of density for divalent or intra-microfibrilar cross-links.

3.2. Beyond the interface failure. The mechanical response of the cross-links

In order to evaluate the mechanical relevance of the cross-links, the analysis should go further the complete failure of the microfibrilar interface. The results in the previous sections show the mechanical role of the interfaces and how its failure can be related with microcracks initiation and the proliferation of damaged zones. Nevertheless, the mechanical behavior of the microfibril beyond the interface failure will be determined by the telopeptide unrolling and further stretching of the cross-links. In this section, we aim to analyze the influence of the cross-links in the mechanical response of the fibril, considering different densities of divalent and trivalent cross-links. Displacement controlled load is applied in the longitudinal direction at the end of the fiber, while the opposite side is fixed.

The analysis performed consider the following cross-links densities: firstly, maintaining the 100% of trivalent cross-links, the content of divalents takes the values 100%, 75%, 50%, 25% and 0%. Secondly, fixing the 100% of divalent cross-links, the values of trivalents density are 75%, 50%, 25% and 0%. In order to reduce the density of every type of cross-links, the elements are randomly deactivated.

The results shown in Figs. 19 and 20 indicate the that trivalent cross-links exert greater influence than divalent, on the mechanical behavior of the fibril.

4. Conclusions and discussion

In the present work, the mechanical response of a representative cell of the mineralized collagen fibril of bone tissue with cohesive interfaces and enzymatic cross links is analyzed by means of the finite element method.

The main objective of the work consists in evaluating the role of interfaces in the mechanical behavior of mineralized collagen fibril when controlled in-plane displacements are applied. We estimate the stiffness loss of the mineralized collagen fibril and analyze the different interface failure modes, associating them with potential locations of microcracks initiation and damage zones. In addition, we aim to study the mechanical contribution of the cross-links beyond the interface failure.

In the model proposed in this work, the collagen matrix is divided into five sub-domains so that five collagen molecules are considered in the representative cell. For each collagen molecule, different stiffness are included depending on the proximity to the

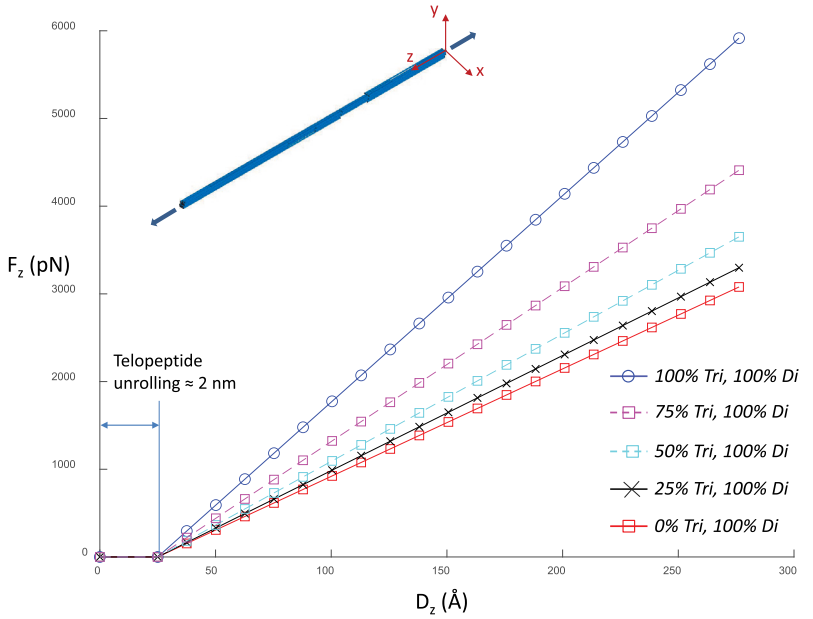

Fig. 20. Evolution of the reaction force F_z (pN) with the displacement applied D_z (Å), considering different values of density for trivalent or inter-microfibrilar cross-links.

mineral and the direction of the applied load, following the work of Shashindra et al. [23]. In the finite element model, the cohesive interfaces aim at reproducing the interactions between the fibril constituents. The mineral-collagen and collagen-collagen interfaces are modeled with cohesive elements with the critical parameters provided by Siegmund et al. [18]. At the same time, the enzymatic cross-links are modeled by considering non-linear springs that can represent the rheological mechanical model proposed by Uzel and Buehler [14] for the C-terminal in collagen type I.

The principal results of this work highlight different failure mechanisms depending on the load case. For the analyzed range of longitudinal controlled elongation, the debonding between mineral and collagen along the boundary normal to the longitudinal fibril direction is the most critical. This agrees with Siegmund et al. [18] although we obtain that the incipient interface failure is delayed when the intermolecular covalent bonds are modeled. For the longitudinal deformation, the cross-links begin to work at $\epsilon_x \approx 0.1$. In addition, the action of the cross-links introduce a balance moment into the collagen molecule that contributes to a delay of the interface failure. The mineral-collagen debonding observed in Fig. 10, leads to a narrow strain that can promote intramicrofibrillar microcracking, whereas collagen-collagen sliding would be related with the presence of damage zone. These results are in agreement with Luo et al. [19], where it was stated that the different interface failure type (depending on its nature) is correlated with different types of microdamage accumulation.

For the load case of controlled transverse elongation the interface failure involves the normal separation between collagen molecules. No significant sliding is observed. For the load case of controlled shear strain, the interface failure is due to collagen molecules sliding.

The results summary provided in Table 3 highlights the stiffness loss of the tissue associated with the different load cases. The quantification of the percentage reduction of the Young's moduli and the shear stiffness when the fibril is deformed, can be useful for applying criteria based on degradation of elastic constants in a larger scale length of bone tissue.

In the work of Hang and Baber [38], the experimental test applied to several mineralized collagen fibrils from antler provides the stress–strain behavior under longitudinal traction load. In that work, an initial region (2–3.7% in deformation) of linear elastic behavior is observed, followed by a second region characterized by a non-linear behavior. In the latter, the deformation is associated with the intermolecular slippage and failure at the mineral collagen interface. For the first region, an average Young's modulus of 2.4 GPa is calculated and for the second region, a noticeable stiffness reduction is observed in several specimens with an average Young's modulus of 1.26 GPa.

The main trend of our results agrees with the work of Hang and Baber [38] regarding the range of linear elastic strain regime and the stiffness loss because of several failure mechanisms. Nevertheless, in the current work, the Young's moduli obtained are greater than in Hang's work because it is known that the mineral content in antler tissue is the lowest of common bone types [39]. Therefore, this can be an important cause of discrepancies. Besides, full mineralization within the fibril is assumed in this work.

In the work of Nair et al. [40], the molecular mechanics of mineralized collagen fibrils is addressed. In that work, stress-controlled longitudinal traction is applied on a 1-D cell (gap and overlap zones). In several points, our results are in agreement with Nair et al. [40]: (1) when the collagen fibril is mineralized, a clear increment in the deformation of the collagen confined in the overlap zone is observed; (2) the maximum stress at the mid-length of the mineral is 3–4 times the maximum stress in the collagen at the overlap zone as our results confirm.

In the work of Buehler [22] the Young's modulus (in longitudinal direction) for the mineralized collagen fibril is 6.23 GPa, the yield strain is 6.7% and the strength to fracture 0.6 GPa. In our results, the Young's modulus for the linear response is estimated as 9.46 GPa and the averaged stiffness modulus including the non-linear response is 6.42 GPa. We have also obtained that the yield strain is 2% and the strength of the interface is 0.6 GPa. In [22] the observed failure mechanism is mainly the collagen-collagen and collagen-mineral sliding rather than the initial collagen-mineral debonding.

In addition, in this work we provide the response in the transverse direction and under shear loading. To the authors' knowledge, neither nano-experimental data of transverse traction nor shear have been found in literature.

From the results obtained, we have related the maximum stress corresponding to the incipient failure of the constituent interface for each load case. The strength achieved in the longitudinal direction of the fibril is more than 20 times greater than the strength in the transverse direction and more than 3.5 times greater than the shear strength.

The simulations, in the two-dimensional model, are performed until the cohesive failure criteria is reached which entails the complete interface failure. Beyond this point, cross-links transfer the load. In this work, a three-dimensional numerical model of the microfibril is generated following Orgel et al. [9] and Alexander et al. [37] including both inter- and intra-microfibrilar cross-links. In concordance with Buehler [16], Uzel and Buehler [14], Barkaoui and Hambli [17], our results reveal that cross-links can transfer the load in the fiber structure at the large strain range, specially when their density increases. Cross-links have very little or negligible effect while interactions in the interfaces between mineral-collagen and collagen molecules, govern the failure mechanisms. Below strain values of 0.1–0.3 (depending on the applied load case), interface failure mechanisms govern the stiffness loss of the mineralized collagen fibril.

Certain bone pathology like osteoporosis, involves important changes in the biochemistry of the collagen molecule such as the change in the cross-links profile. The reduction of the trivalent cross-links (inter-microfibrilar) in favor of divalents has been observed in osteoporosis specimens, entailing a high loss of the mechanical competence of bone [12]. Results obtained in this work confirm that trivalent cross-links present more impact than divalent, on the stiffness of the fibril.

CRediT authorship contribution statement

Ana Vercher-Martínez: Writing – original draft, Software, Methodology, Funding acquisition, Conceptualization. **Eugenio Giner:** Writing – review & editing, Funding acquisition, Formal analysis. **F. Javier Fuenmayor:** Writing – review & editing, Funding acquisition, Formal analysis. **J. Manuel García-Aznar:** Conceptualization.

Declaration of competing interest

The authors declare that they have no known conflict of interests or personal relationships in the present work.

Data availability

No data was used for the research described in the article.

Acknowledgments

The authors acknowledge the Ministerio de Ciencia e Innovación y Universidades and the European Regional Development Fund (FEDER) for the financial support received through the projects PID2020-118920RB-I00, PID2020-118480RB-C21 and C22 funded by MCIN/AEI/10.13039/501100011033 and by "ERDF A way of making Europe", the Ministerio de Ciencia e Innovación y Universidades MCIN/AEI/10.13039/501100011033 and Europe Union Next Generation EU/PRTR for the projects PDC2021-121368-C21 and C22, CRUE-Universitat Politècnica de València and the Generalitat Valenciana for Programa PROMETEO/2021/046.

References

[1] Liu Y, Kim YK, Dai L, Li N, Khan SO, Pashley DH, et al. Hierarchical and non-hierarchical mineralization of collagen. Biomaterials 2011;32:1291–300.
[2] Balasubramanian P, Prabhakaran MP, Sireesha M, Ramakrishna S. Collagen in hyman tissues: structure, functions and biomedical implications from a tissue engineering perspective. Adv Polym Sci 2013;251:173–206.
[3] Vercher A, Giner E, Arango C, Fuenmayor FJ. Influence of the mineral staggering on the elastic properties of the mineralized collagen fibril in lamellar bone. J Mech Behav Biomed Mater 2015;42:243–56.
[4] Hodge AJ, Petruska JA. Recent studies with the electron microscope on ordered aggregates of the tropocollagen macromolecule. In: Ramachandran GN, editor. Aspects of Protein Structure. New York: Academic Press; 1963, p. 289–300.
[5] Weiner S, Traub W. Organization of hydroxiapatite within collagen fibrils. FEBS Lett 1986;206:262–6.
[6] Landis WJ, Song MJ, Leith A, McEwen L, McEwen BF. Mineral and organic matrix interaction in normally calcifying tendon visualized in three dimensions by high-voltage electron microscopic tomography and graphic image reconstruction. J Struct Biol 1993;110:39–54.
[7] Rho JY, Kuhn-Spearing L, Zioupos P. Mechanical properties and the hierarchical structure of bone. Med Eng Phys 1998;20:92–102.
[8] Orgel JPRO, Miller A, Irving TC, Fischetti RF, Hammersley AP, Wess TJ. The in situ supermolecular structure of type I collagen. Structure 2001;9:1061–9.
[9] Orgel JPRO, Irving TC, Miller A, Wess TJ. Microfibrillar structure of type I collagn in situ. Proc Natl Acad Sci USA 2006;103:9001–5.
[10] Gautier A, Vesentini S, Redaelli A, Buehler MJ. Hierarchical structure and nanomechanics of collagen microfibrils from the atomistic scale up. Nano Lett 2011;11:757–66.
[11] Knott L, Bailey AJ. Collagen cross-links in mineralized tissues: A review of their chemestry, function, and clinical relevance. Bone 1998;22:181–7.
[12] Knott L, Whitehead CC, Fleming RH, Bailey AJ. Biochemical changes in the collageneous matrix of osteoporotic avian bone. Biochem J 1995;310:1045–51.
[13] Eyre DR, Wu J. Collagen cross-links. Top Curr Chem 2005;247:207–29.

[14] Uzel SGM, Buehler MJ. Molecular structure, mechanical behavior and failure mechanism of the C-terminal cross-link domain in type I collagen. J Mech Behav Biomed Mater 2011;4:153–61.
[15] Bailey AJ. Molecular mechanisms of ageing in connective tissue. Mech Ageing Dev 2000;122:735–55.
[16] Buehler M. Nanomechanics of collagen fibrils under varying cross-link densities: Atomistic and continumm studies. J Mech Behav Biomed Mater 2008;1:59–67.
[17] Barkaoui A, Hambli R. Nanomechanical properties of mineralised collagen microfibrils based on finite element method: biomechanical role of cross-links. Comput Methods Biomech Biomed Eng 2013. http://dx.doi.org/10.1080/10255842.2012.758255.
[18] Siegmund T, Matthew RA, Burr DB. Failure of mineralized collagen fibrils. Modelling the role of collagen crosss-linking. J Biomech 2008;41:1427–35.
[19] Luo Q, Nakade R, Dong X, Rong Q, Wang X. Effect of mineral-collagen interfacial behavior on the microdamage progression in bone using a probabilistic cohesive finite element model. J Mech Behav Biomed Mater 2011;4:943–52.
[20] Hamed E, Jasiuk I. Multiscale damage and strength of lamellar bone modeled by cohesive finite elements. J Mech Behav Biomed Mater 2013;28:94–110.
[21] Yan Y, Nakatani A. Stability controlled crack initiation in nacre-like composite materials. J Mech Phys Solids 2019;125:591–612.
[22] Buehler M. Molecular nanomechanics of nascent bone: fibrillar toughening by mineralization. Nanotechnology 2007;18:295102, 9.
[23] Shashindra MP, Kalpana SK, Dinesh RK. Multiscale model of collagen fibril in bone: elastic response. J Eng Mech 2014;140:454–61.
[24] Depalle B, Qin Z, Shefelbine SJ, Buehler M. Influence of cross-link structure, density and mechanical properties in the mesoscale deformation mechanisms of collagen fibrils. J Mech Behav Biomed Mater 2015;52:1–13.
[25] Hamed E, Jasiuk I. Elastic modeling of bone at nanostructural level. Mater Sci Eng 2012;73:27–49.
[26] Fritsch A, Hellmich C, Dormieux L. Ductile sliding between mineral crystals followed by rupture of collagen crosslinks: Experimental supported micromechanical explanation of bone strength. J Theoret Biol 2009;260:230–52.
[27] Vercher A, Giner E, Arango C, Tarancón JE, Fuenmayor FJ. Homogenized stiffness matrices for mineralized collagen fibrils and lamellar bone using unit cell finite element models. Biomech Model Mechanobiol 2014;13:437–49.
[28] Yuan F, Stock SR, Haeffner DR, Almer JD, Dunand DC, Brinson LC. A new model to simulate the elastic properties of mineralized collagen fibril. Biomech Model Mechanobiol 2011;10:147–60.
[29] Silver FH, Landis WJ. Deposition of apatite in mineralizing vertebrate extracellular matrices: A model of possible nucleation sites on type I collagen. Connect Tissue Res 2011;52:242–54.
[30] Landis WJ, Song MJ. Early mineral deposition in calcifying tendon characterized by high voltage electron microscopy and three-dimensional graphic imaging. J Struct Biol 1991;107:116–27.
[31] Landis WJ, Silver FH. The structure and function of normally mineralized avian tendons. Comp Biochem Physiol Part A 2002;133:1135–57.
[32] Martínez-Reina J, Domínguez J, García-Aznar JM. Effect of porosity and mineral content on the elastic constants of cortical bone: a multiscale approach. Biomech Model Mechanobiol 2011;10:309–22.
[33] Buehler M. Atomistic and continuum modeling of mechanical properties of collagen: Elasticity, fracture, and self-assembly. J Mater Res 2006;21:1947–61.
[34] Gao YF, Bower AF. A simple technique for avoiding convergence problems in finite element simulations of crack nucleation and growth on cohesive interfaces. Modelling Simul Mater Sci Eng 2004;12:453–63.
[35] Xu XP, Needleman A. Numerical simulation of fast cracl growth in brittle solids. J Mech Phys Solids 1994;42:1397–415.
[36] Beyer MK. The mechanical strength of a covalent bond calculated by density functional theory. J Chem Phys 2000;112:7307–12.
[37] Alexander B, Daulton TL, Genin GM, Lipner J, Pasteris JD, Wopenka B, et al. The nanometre-scale physiology of bone: steric modelling and scanning transmission electron microscopy of collagen?mineral structure. J R Soc Interface 2012;19:1774–86.
[38] Hang F, Baber AH. Nano-mechanical properties of individual mineralized collagen fibrils from bone tissue. J R Soc Interface 2011;8:500–5.
[39] Gupta HS, Krauss S, Kerschmitzki M, Karunaratne A, Dunlop JWC, Barber AH, et al. Intrafibrillar plasticity through mineral/collagen sliding is the dominant mechanism for the extreme toughness of antler bone. J Mech Behav Biomed Mater 2013;28:366–82.
[40] Nair AK, Gautier A, Chang SW, Buheler MJ. Molecular mechanics of minerlized collagen fibrils in bone. Nature Commun 2013;4:1724. http://dx.doi.org/10.1038/ncomms2720.